A Benchmark for the Number of Independent Line of Sight Links on a Given Volume Platform

Ozzola, Riccardo; Cavallo, Daniele; Freni, Angelo; Llombart, Nuria; Neto, Andrea

DOI
10.1109/TAP.2022.3209203

Publication date
2022

Document Version
Final published version

Published in
IEEE Transactions on Antennas and Propagation

Citation (APA)
Ozzola, R., Cavallo, D., Freni, A., Llombart, N., & Neto, A. (2022). A Benchmark for the Number of Independent Line of Sight Links on a Given Volume Platform. *IEEE Transactions on Antennas and Propagation*, *70*(12), 12071-12080. https://doi.org/10.1109/TAP.2022.3209203

A Benchmark for the Number of Independent Line of Sight Links on a Given Volume Platform

Riccardo Ozzola, *Graduate Student Member, IEEE*, Daniele Cavallo, *Senior Member, IEEE*, Angelo Freni, *Senior Member, IEEE*, Nuria Llombart, *Fellow, IEEE*, and Andrea Neto, *Fellow, IEEE*

***Abstract*— The number of independent links that can be hosted by an antenna platform for line-of-sight (LoS) communications is limited by its physical size and the interference between the beams associated with different users. For large-size platforms, the interference can be reduced by compromising the aperture efficiency, and this tradeoff is the metric to quantify the effective use of the platform. This metric fails for antenna platforms that are not electrically large, for which the aperture efficiency is no longer a useful parameter. Here we resort to the concept of the observable field, related to the maximum theoretical directivity, to estimate the potential number of independent links supported by moderate-size platforms. This allows the introduction of coupling coefficients between the beams associated with the observable portion of the incident field and the beams associated with the receiving antennas. These coefficients are bounded to unity for any platform dimension, unlike the aperture efficiency, and they are maximized when the antenna pattern is equal to the pattern predicted by the observable field. Accordingly, selecting beams dictated by the observable field constitutes a benchmark for the effective use of the volume. Any antenna design can be compared to this benchmark to assess its merits.**

***Index Terms*— Interference, line of sight (LoS), multi-beam antennas, observable field, signal-to-interference ratio (SIR).**

I. Introduction

THE next generation of wireless communication systems [1], [2] will soon require multi-beam antenna system capabilities [3], [4], similar to those employed in satellite-based communication [5], [6], [7], [8], [9]. In these systems, the efficient use of the platform volume is a significant challenge, especially for the lower frequency bands. This issue has been recently recognized as significant also by the telecommunication industry [10]. However, it had been anticipated by the scientific community with the original studies on the degrees of freedom of the field [11], [12], or in the related electromagnetic multiple-input and multiple-output (MIMO) scientific community [13], [14]. In this contribution, the emphasis is posed on line-of-sight (LoS) communication scenarios, where several beams corresponding to different data streams are directed toward the antenna platform (see Fig. 1). The beams from the users can be plane waves, e.g., for far-field links, or, more generally, spectra of multiple plane waves, e.g., for near-field communication scenarios. For a given link, its data stream corresponds to the desired signal, while the other data streams interfere. Links are assumed to be independent if the signal to interference ratio (SIR) remains above a predefined threshold. It is known that the mutual coupling between the beams limits the maximum number of independent beams hosted by a platform [15].

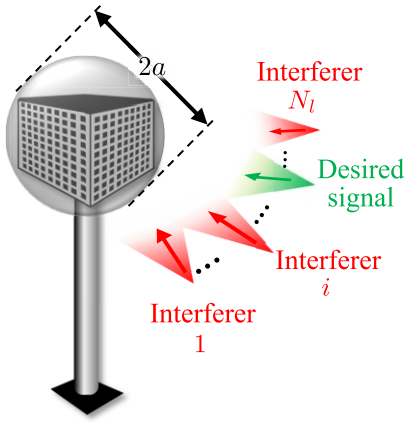

Fig. 1. Depiction of a multi-beam LoS scenario with N_l simultaneous links, each associated with an incident beam.

Satellite-based multi-beam communications mainly use aperture antennas that are large in terms of wavelength. Thus, the aperture efficiency is the main parameter to consider. Tapering the aperture distribution leads to lower sidelobes at the cost of beam widening and aperture efficiency reduction. However, the aperture efficiency concept, defined for electrically large antennas, cannot be applied for antennas whose size is comparable with the wavelength. Accordingly, to date, an appropriate metric to state how many independent links can be established on a platform of moderate size does not exist. To define such a metric, one needs to know how much power an antenna with a given radiation pattern can receive. For this purpose, this article exploits the concept of

Manuscript received 3 January 2022; revised 30 May 2022; accepted 4 September 2022. Date of publication 30 September 2022; date of current version 22 December 2022. This work was supported by HUAWEI Technologies Sweden AB, UNB Project, under Grant YBN2020045031. *(Corresponding author: Riccardo Ozzola.)*

Riccardo Ozzola, Daniele Cavallo, Nuria Llombart, and Andrea Neto are with the THz Sensing Group, Microelectronics Department, Delft University of Technology, 2628 CD Delft, The Netherlands (e-mail: r.ozzola-1@tudelft.nl).

Angelo Freni is with the Dipartimento di Ingegneria dell'Informazione, University of Florence, 50139 Florence, Italy.

Color versions of one or more figures in this article are available at https://doi.org/10.1109/TAP.2022.3209203.

Digital Object Identifier 10.1109/TAP.2022.3209203

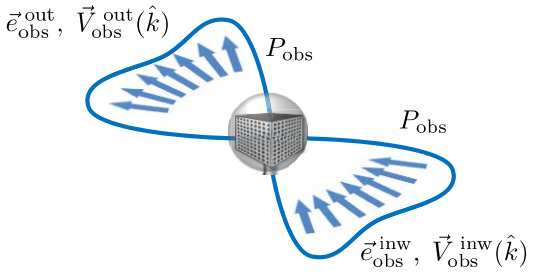

Fig. 2. Pictorial representation of the inward and outward components of the observable field associated with the sphere of radius a enclosing the base station platform.

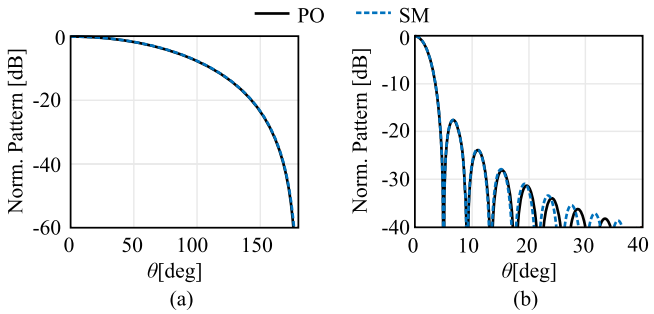

Fig. 3. Observable field patterns for spherical antenna domains of radius. (a) $a = 0.02\lambda_0$ and (b) $a = 7\lambda_0$.

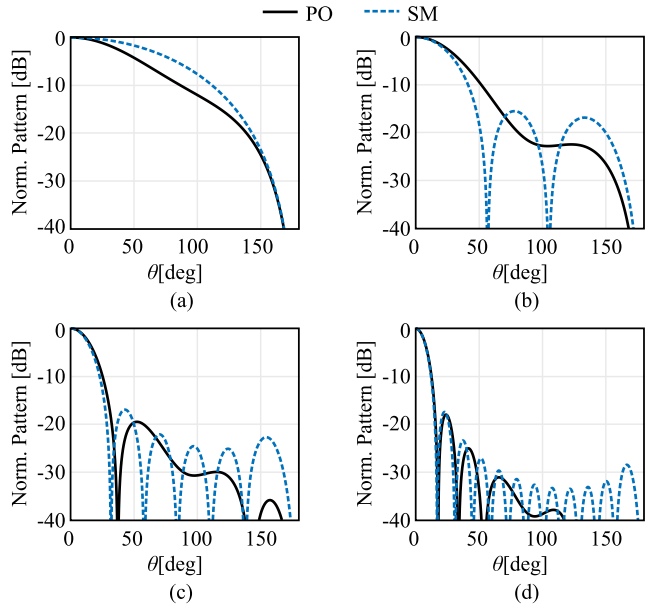

Fig. 4. Observable field patterns for small to moderate spherical antenna domains of radius. (a) $a = 0.3\lambda_0$, (b) $a = 0.5\lambda_0$, (c) $a = \lambda_0$, and (d) $a = 2\lambda_0$.

the observable field [16] to represent the portion of the incident field that can be received. This allows the introduction of a novel coupling coefficient, which correlates the observable field and the pattern under investigation. The square magnitude of this coefficient represents the fraction of the maximum power the antenna bounded by a given volume can receive. If one or more interferers are present, one can express the SIR using the introduced coupling coefficient. This allows us to study several antenna aperture distributions compatible with the antenna volume, regardless of the specific antenna design. The proposed methodology constitutes a useful tool to relate the SIR to the antenna dimensions, aperture distribution, and the number of simultaneous independent links.

This article is organized as follows. In Section II, the concept of the observable field is recalled, and two different approaches for its evaluation are compared. In Section III, the novel coupling coefficients are defined, and the expression of the SIR through these coefficients is introduced. In Section IV, a benchmark situation is established and used to assess some preliminary antenna dimensioning. In Section V, the SIR versus the number of links is evaluated for fixed-size platforms. Conclusions are drawn in Section VI.

II. Observable Field Patterns

For antennas whose dimensions are comparable with the wavelength, we resort to the concept of the observable field [16], [17] and its associated observable power $P_{\rm obs}$, which is the maximum power that can be received by an antenna enclosed in a given spherical volume of radius a. The observable field, depicted in Fig. 2, can be expressed as the superposition of an inward and an outward propagating waves

$$\vec{e}_{\rm obs}(\vec{r}) = \vec{e}_{\rm obs}^{\,\rm inw}(\vec{r}) + \vec{e}_{\rm obs}^{\,\rm out}(\vec{r}) \tag{1}$$

where $\vec{r} = (r, \theta, \phi)$ is a point in the far-field region of the antenna domain. Both terms are characterized by an angular pattern $\vec{V}_{\rm obs}^{\,\rm inw/out}$ and a spherical spreading

$$\vec{e}_{\rm obs}^{\,\rm inw/out}(\vec{r}) = \vec{V}_{\rm obs}^{\,\rm inw/out}(\hat{k})\frac{e^{\pm jkr}}{r} \tag{2}$$

where the separation of the spatial variables r, θ, ϕ is used, and $\hat{k}$ is defined as $\hat{k} = \sin\theta\cos\phi\hat{x} + \sin\theta\sin\phi\hat{y} + \cos\theta\hat{z}$. The "classic" procedure to define the observable field resorts to a spherical mode (SM) expansion of the incident field [18], [19] and retains only the first $N_{\rm sp} < ka$ modes, where k is the free-space wavenumber. An alternative representation is based on the physical optics (PO) currents and was proposed in [16] and [17]. It resorts to spatial windowing to select the equivalent currents distributed on the surface enclosing the finite domain under analysis: these currents radiate the outward component of the observable field.

Fig. 3 shows the observable far-field patterns evaluated using both the PO and the SM procedures for $a = 0.02\lambda_0$ and for $a = 7\lambda_0$. The PO and SM curves coincide for the smaller radius case [see Fig. 3(a)], while they are very similar up to the fourth sidelobe for the larger antenna case [see Fig. 3(b)]. However, for antenna dimensions comparable with the wavelength, the two procedures give origin to significantly different patterns. In Fig. 4, the observable field patterns are reported for different radii a. It is apparent that, for these intermediate platform sizes, the SM observable field patterns are characterized by a higher number of nulls (equal to the number of modes $N_{\rm sp}$) than the PO patterns. Moreover, the SM pattern changes in a quantized manner, related to the discrete number of retained modes $N_{\rm sp}$. On the contrary, the PO observable field has patterns that change in a continuous way with respect to size.

III. Received Signals in Terms of Observable Field

In this section, we use the observable field to evaluate the beam coupling for a receiving antenna, introducing new coefficients.

A. Introduction of the Reception Coupling Coefficient

Let us consider the receiving platform enclosed by the minimum spherical volume of radius a, as shown in Fig. 1. Assume that N_l sources are located in different positions, and they are all in the far-field with respect to the antenna platform, which results in N_l plane waves reaching the receiving antenna. Following the procedure in [16] and [17] or using the SM expansion [19], the observable field can be calculated for the ith wave impinging from the direction $\hat{k}_i$. Correspondingly, the associated power can be indicated as P^i_{obs}. The capability of a specific antenna, contained in a spherical volume of radius a and pointing to the $\hat{k}_j$ direction, to receive the wave impinging from the direction $\hat{k}_i$ can be expressed by defining a reception coupling coefficient $C^{ij}_{\text{obs,a}}$ as

$$P^{ij}_{\text{r}} = P^i_{\text{obs}} \left| C^{ij}_{\text{obs,a}} \right|^2 \tag{3}$$

where $C^{ij}_{\text{obs,a}}$ is the coupling coefficient between the observable field of the incident beams $\vec{V}^{\text{inw}}_{\text{obs},i}(\hat{k})$ and the pattern of the receiving antenna $\vec{V}^j_{\text{a}}(\hat{k})$. To calculate $C^{ij}_{\text{obs,a}}$, one can first express the received power for the jth antenna under conjugate matching conditions, following the procedure reported in Appendix A, as:

$$P^{ij}_{\text{r}} = \frac{\left| V^{ij}_{oc} I^j_{\text{a}} \right|^2}{16 P^j_{\text{a}}} \tag{4}$$

where V^{ij}_{oc} is the open-circuit voltage at the input terminals of the receiving jth antenna when the ith wave is impinging, and P^j_{a} is the power radiated by the jth antenna when operated in transmission, fed by the input current I^j_{a}. The product $V^{ij}_{oc} I^j_{\text{a}}$ can be interpreted as the reaction between the observable field associated with the direction i and the source feeding the jth antenna, as described in Appendix B, where we made use of Lorentz's reciprocity theorem [20], [21], [23], [24]. Comparing (3) with (4), we can define the coupling coefficient as follows:

$$C^{ij}_{\text{obs,a}} = \frac{V^{ij}_{oc} I^j_{\text{a}}}{4\sqrt{P^j_{\text{a}} P^i_{\text{obs}}}}. \tag{5}$$

In particular, (5) can be evaluated by exploiting the reciprocity theorem. As shown in Appendix B, when the ith interfering source and the antenna are at a far-field distance, we have

$$V^{ij}_{oc} I^j_{\text{a}} = \frac{2}{\zeta} \iint_{4\pi} \vec{V}^{\text{inw},i}_{\text{obs}}(\hat{k}) \cdot \vec{V}^j_{\text{a}}(\hat{k}) d\hat{k} \tag{6}$$

where $\vec{V}^j_{\text{a}}$ is the angular pattern of the electric field $\vec{e}^j_{\text{a}}(\vec{r})$ radiated by the receiving antenna, when operated in transmission and fed in such a way as to generate the jth beam, i.e.,

$$\vec{e}^j_{\text{a}}(\vec{r}) = \vec{V}^j_{\text{a}}(\hat{k}) \frac{e^{-jkr}}{r}. \tag{7}$$

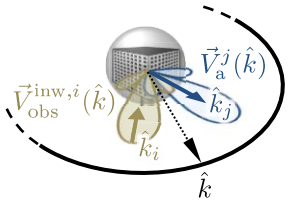

Fig. 5. Depiction of the antenna and observable field patterns used for the calculations of the $\hat{k}$-integrals in (6) and (9).

The terms appearing in (6) are described in Fig. 5, which shows the outward antenna pattern pointing toward $\hat{k}_j$, the inward observable field pattern from the direction $\hat{k}_i$, and the integration variable $\hat{k}$ spanning the entire solid angle for the calculation of the coupling integral. The observable power and the power radiated by the receiving antenna can be expressed as follows:

$$\begin{aligned} P^i_{\text{obs}} &= \frac{1}{2\zeta} \iint_{4\pi} \left| \vec{V}^{\text{inw},i}_{\text{obs}}(\hat{k}) \right|^2 d\hat{k} \\ P^j_{\text{a}} &= \frac{1}{2\zeta} \iint_{4\pi} \left| \vec{V}^j_{\text{a}}(\hat{k}) \right|^2 d\hat{k} \end{aligned} \tag{8}$$

substituting (6) and (8) in (5) leads to

$$C^{ij}_{\text{obs,a}} = \frac{\iint_{4\pi} \vec{V}^{\text{inw},i}_{\text{obs}}(\hat{k}) \cdot \vec{V}^j_{\text{a}}(\hat{k}) d\hat{k}}{\sqrt{\iint_{4\pi} \left| \vec{V}^{\text{inw},i}_{\text{obs}}(\hat{k}) \right|^2 d\hat{k} \iint_{4\pi} \left| \vec{V}^j_{\text{a}}(\hat{k}) \right|^2 d\hat{k}}}. \tag{9}$$

The above coefficients represent the counterpart of Stein's coefficients [15], which are defined for two beams of the same transmitting antenna. It is worth mentioning that the definition of the coupling coefficients in (9) is independent of the specific method used to evaluate the observable field and that $|C^{ij}_{\text{obs,a}}| \leq 1$. In the case of $i = j$, the coefficient $C^{jj}_{\text{obs,a}}$ is the coupling with the desired beam. The upper limit $|C^{ij}_{\text{obs,a}}| = 1$ is achieved when the outward pattern of the receiving antenna is chosen to be equal to the inward pattern of the observable field, i.e., $\vec{V}^j_{\text{a}}(\hat{k}) = \vec{V}^{\text{inw},j}_{\text{obs}}(\hat{k})$. Under this condition, the received power is maximized.

B. Evaluation of the Desired Received Signals

In a multi-link communication scenario, one can assume that the incident field is the superposition of N_l links, where one is desired and the remaining $N_l - 1$ are the interferers. Each link is characterized by a unit vector direction $\hat{e}_i$ for the electric field, an amplitude E_i, and a direction of propagation $\hat{k}_i$. We can assume that the waves incident from different directions are uncorrelated, and they have the same amplitude, i.e., $E_i = E_0$, $\forall i$. Accordingly, the expected total power received at the jth antenna can be expressed as follows:

$$P^j_{\text{r}} = \sum_{i=1}^{N_l} P^i_{\text{obs}} \left| C^{ij}_{\text{obs,a}} \right|^2 = P^{\text{pw}}_{\text{obs}} \sum_{i=1}^{N_l} \left| C^{ij}_{\text{obs,a}} \right|^2. \tag{10}$$

It is worth noting that $P^i_{\text{obs}} = P^{\text{pw}}_{\text{obs}} \forall i$ since we have considered the same excitation for all the directions, and since the observable power does not depend on the direction $\hat{k}_i$.

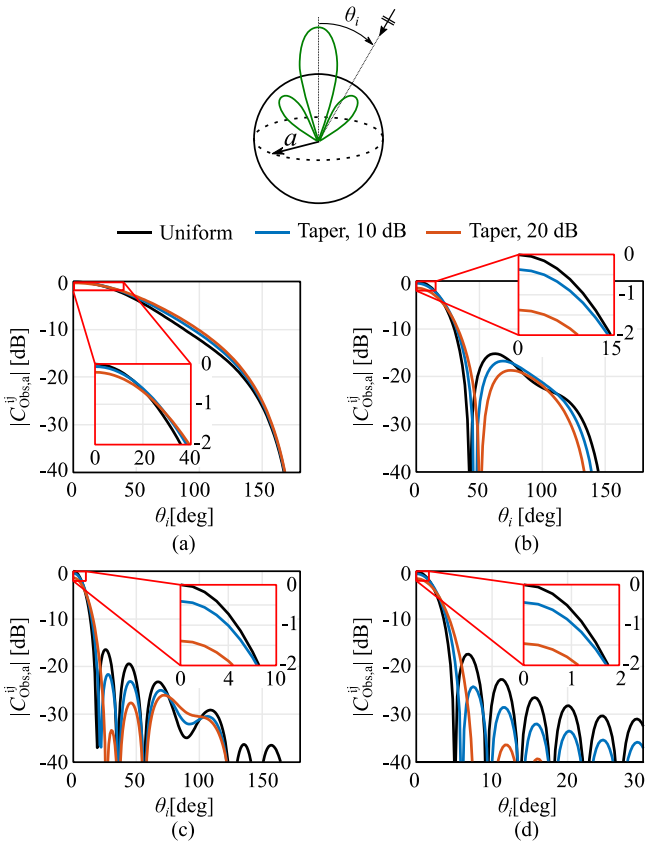

Fig. 6. Coupling coefficients between the observable field and the antenna pattern $\vec{V}_{\mathrm{a}}$ with different excitations for radii. (a) $a = 0.5\lambda_0$, (b) $a = \lambda_0$, (c) $a = 2\lambda_0$, and (d) $a = 7\lambda_0$.

By resorting to the coupling coefficients, the expected power of the desired signal can be expressed as follows:

$$S_j = P^{\mathrm{pw}}_{\mathrm{obs}} \left| C^{jj}_{\mathrm{obs,a}} \right|^2. \tag{11}$$

Using a tapered illumination makes it possible to reduce interference by lowering the sidelobe level (SLL). However, given the antenna dimension, the use of the taper reduces $|C^{jj}_{\mathrm{obs,a}}|$, yielding a reduction of the received power of the desired signal. While the theory developed until now is valid for generic beams, the examples in this contribution are specialized to the case in which the incident beams are plane waves. In the example addressed in Fig. 6, the values of $|C^{ij}_{\mathrm{obs,a}}|$ are calculated for a family of antenna patterns $\vec{V}^{\,j}_{\mathrm{a}}(\hat{k})$, whose radiation is centered at the broadside. The coefficients $|C^{ij}_{\mathrm{obs,a}}|$ are plotted versus θ_i, i.e., the direction of incidence of the ith signal. The specific antenna patterns $\vec{V}^{\,j}_{\mathrm{a}}(\hat{k})$ are derived from $\vec{V}^{\,j}_{\mathrm{a}}(\hat{k}) = \vec{V}^{\mathrm{inw},j}_{\mathrm{obs}}(\hat{k})$ or by applying different Gaussian tapers, following the formalism of [22]. For the uniform case, it appears that $|C^{ij}_{\mathrm{obs,a}}(0)| = 1$, as the maximum coupling to the incident plane wave is achieved. The taper has almost negligible effects for small antennas, while, for radii $a > \lambda_0$, the tapering yields a lower coupling from the side lobes and an evident reduction of the $|C^{jj}_{\mathrm{obs,a}}|$ around $\theta = 0°$. In particular, $|C^{ij}_{\mathrm{obs}}(0)|^2 \approx 0.92$ and ≈ 0.72, for the 10 and the 20 dB taper, respectively.

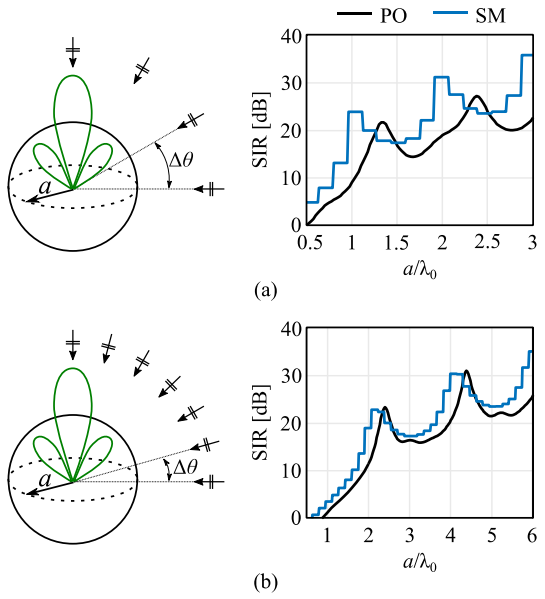

Fig. 7. SIR versus the radius of the sphere enclosing the antenna for N_I interferers located on the same plane, and spaced by $\Delta\theta$. (a) $\Delta\theta = 30°$ and $N_I = 4$, (b) $\Delta\theta = 15°$ and $N_I = 7$.

C. Evaluation of the SIR

By using the coupling coefficients, the interference at the jth antenna becomes as follows:

$$I_j = P^{\mathrm{pw}}_{\mathrm{obs}} \sum_{\substack{i=1 \\ i \neq j}}^{N_I} \left| C^{ij}_{\mathrm{obs,a}} \right|^2 \tag{12}$$

and, consequently, the SIR can be expressed as

$$\frac{S_j}{I_j} = \frac{\left| C^{jj}_{\mathrm{obs,a}} \right|^2}{\sum_{\substack{i=1 \\ i \neq j}}^{N_I} \left| C^{ij}_{\mathrm{obs,a}} \right|^2}. \tag{13}$$

In Fig. 7, the SIR for a configuration with N_I users distributed at equispaced fixed directions in the range from 0° to 90° is investigated for $\vec{V}^{\,j}_{\mathrm{a}}(\hat{k}) = \vec{V}^{\mathrm{out},j}_{\mathrm{obs}}(\hat{k})$. SM and PO methodologies are compared for their prediction of interference. Between the methodologies, we can note that the PO approach gives lower SIR values. However, both show oscillations around a monotonic increase of the SIR versus the antenna radius. The oscillations indicate that for any given link spacing $\Delta\theta$, specific antenna dimensions can enhance the SIR. The curves show a low SIR for electrically small antenna domains due to the relatively broad beam. When the domain occupied by the antenna becomes larger, the main beam becomes narrower, and the interferers contribute via the antenna side lobes only. Consequently, the SIR increases. It can be noted that the SM method presents a stepped behavior, and its peaks are overestimated if compared with the PO method.

IV. Properties of the SIR With Respect to the Minimum Sphere Radius

In this section, a benchmark study is presented in order to estimate the maximum number of independent links supported

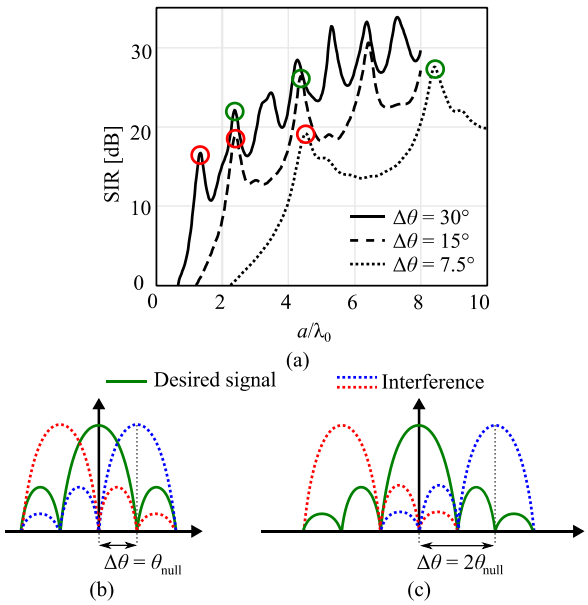

Fig. 8. (a) SIR in case of uniform aperture distributions, benchmark, for users uniformly distributed on the FoV, where $\Delta\theta$ is the separation angle between the users. The first and second peaks of each curve are highlighted in red and green, respectively. Beams and interferers: (b) first interferer on the first null, and (c) first interferer at $2\theta_{null}$.

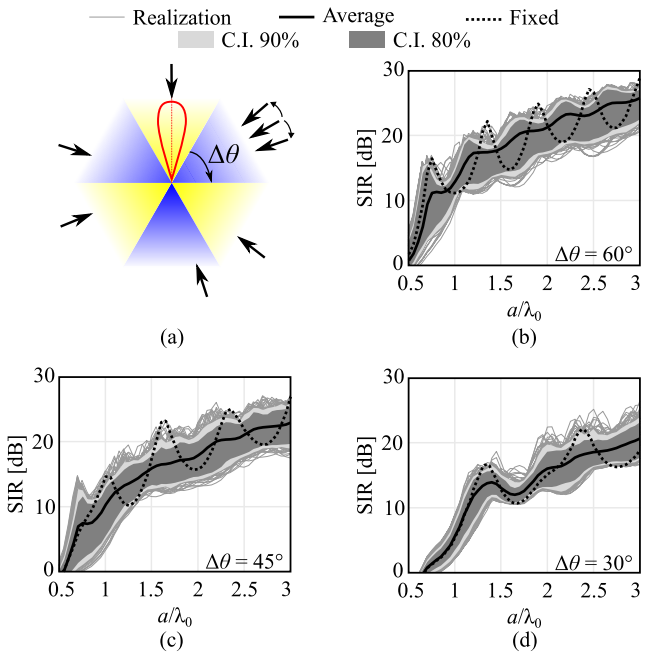

Fig. 9. (a) Communication scenario with moving interferers and main beam aligned with the desired signal, and its corresponding SIR obtained with the benchmark illumination for (b) $\Delta\theta = 60°$, (c) $\Delta\theta = 45°$, and (d) $\Delta\theta = 30°$ spacing.

by a platform of finite dimensions. Since the PO methodology produces systematically more conservative and not quantized SIR values, in the following, we will maintain our attention on the PO methodology only. As before, we assume that the main beam is aligned with the desired signal, while the interferers are located in fixed directions or allowed to be randomly moved within an angular sector. Specifically, the scenario we are considering consists of several users spread around the base station on a 360° field of view (FoV), where the receiving antenna is located. Polarization matching is considered for interference to analyze the worst case.

A. Benchmark With the PO Currents

The case $\vec{V}_a^j(\hat{k}) = \vec{V}_{obs}^{out,j}(\hat{k})$ is referred to as the "benchmark." Fig. 8(a) shows the SIR for fixed interferers uniformly separated by $\Delta\theta$. For a larger number of interferers, resulting from smaller $\Delta\theta = 30°, 15°, 7.5°$, the SIR curves shift and stretch to the right. It can be noted that the first peak always corresponds to $a \approx 35\lambda_0/\Delta\theta$, and its value is ≈18 dB. For such a dimension a, the main beam of this benchmark uniform case has its first null at $\theta_{null} \approx \Delta\theta$. Thus, the first peak occurs when the interferer closest to the signal direction is aligned with the first null of the pattern [see Fig. 8(b)].

From the curves in Fig. 8(a), one can easily determine a bandwidth around the peak over which the SIR remains higher than a threshold level. For instance, if the purpose is to serve 24 equispaced users on a 360° FoV with SIR > 15 dB, for $\Delta\theta = 15°$ in Fig. 8(a), one can select an antenna domain of radius $a = 2.3\lambda_0$, implement a uniform current distribution, and expect that the desired SIR is guaranteed over about 13% bandwidth. An equivalent bandwidth can also be found for the other values of $\Delta\theta$. It may be useful to extend this simple reasoning to all $\Delta\theta$ and assume that the minimum threshold to consider independent links to be SIR > 14 dB. A simple rule for the number of equispaced users in an FoV expressed in degrees can then be derived for the benchmark distribution

$$N_{14dB}^{equi} = \text{FoV}\frac{a}{35\lambda_0}. \tag{14}$$

The second peak of the curves of Fig. 8(a) corresponds to the configuration of the non-overlapping beams shown in Fig. 8(c), where the first interferer is aligned with the second null of the antenna pattern.

In the following, we consider that each interferer is randomly located in an angular sector $\Delta\theta$ wide, as sketched in Fig. 9(a). Since each interferer is randomly located in a sector, a Monte Carlo analysis has been performed, considering the interferer uniformly distributed in $\Delta\theta$. Fig. 9(b) shows the SIR corresponding to 250 realizations for $\Delta\theta = 60°$, and assuming the benchmark distribution. In the plot, the average SIR, the SIR in the case of fixed and equispaced positions of the users, and the 80% (dark gray area) and the 90% (light gray area) confidence intervals are also reported. Looking at the confidence intervals in Fig. 9, we can notice that they interpolate the maxima and minima of the oscillating fixed-user SIR. Fig. 10(c) and (d) presents the same analysis for $\Delta\theta = 45°$ and $\Delta\theta = 30°$, respectively. In the last two cases, since the interferers are angularly closer, the SIR is about 3 and 6 dB lower, respectively, compared with $\Delta\theta = 60°$. The confidence interval is also narrower since the interferers are distributed randomly within a smaller pertinent sector.

B. Analysis of the Aperture Distribution Taper

Once the benchmark for the SIR has been assessed, one can investigate the potential increases of SIR deriving from the

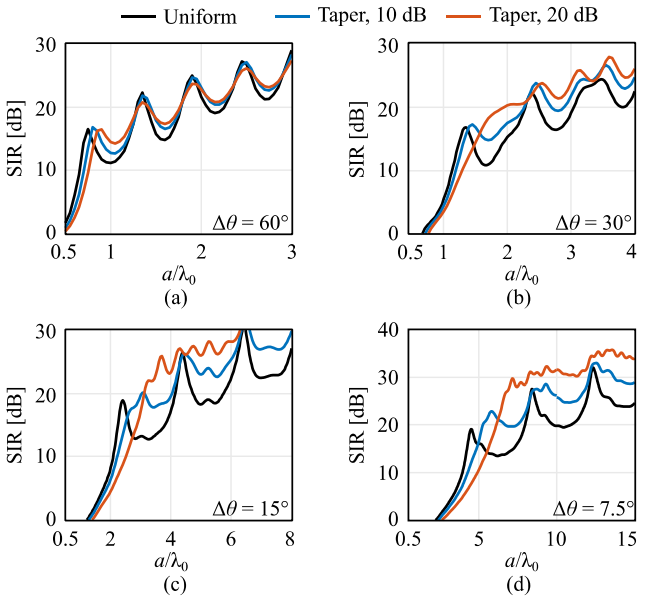

Fig. 10. SIR comparison between a uniform distribution, a 10 dB Gaussian taper, and a 20 dB Gaussian taper for equispaced beams with (a) $\Delta\theta = 60°$, (b) $\Delta\theta = 30°$, (c) $\Delta\theta = 15°$, and (d) $\Delta\theta = 7.5°$.

use of a tapered aperture distribution, which for large antenna volumes compromises the main beam efficiency for lower side lobes. Fig. 10 shows the SIR for the equispaced fixed users in the case of four different values of $\Delta\theta$: 60°, 30°, 15°, and 7.5°, which correspond to N_l: 6, 12, 24, and 48. In all cases, the taper leads to wider main lobes and to a $|C_{\text{obs,a}}| < 1$. For larger radii, the patterns of the tapered distribution are characterized by lower sidelobes, which result in smaller oscillations of the SIR, compared to the uniform distribution. On the contrary, for small domains, specifically for $a < 35\lambda_0/\Delta\theta$, the taper reduces the SIR.

Fig. 11 shows the SIR in the case of randomly distributed interferers for several angular sectors $\Delta\theta$ and different aperture distribution tapers. Compared with the benchmark uniform distribution case, the confidence intervals associated with tapered distributions become significantly narrower for large radii of the minimum sphere enclosing the antenna (see Fig. 9). For smaller radii instead, the confidence intervals become broader than in the absence of tapering. That is because the main beam of the antennas becomes wider, and especially for $\Delta\theta = 45°$, the interferers are associated with beams that can arrive from directions relatively close to the main beam.

V. Number of Links for Fixed-Size Platforms

A useful operative parameter that can be used to assess the properties of a platform of fixed radius a is the number of links supported with an SIR larger than a predefined threshold. Fig. 12 shows the SIR versus the number of links, or equivalently the spacing $\Delta\theta$, for platforms of radius $a = \lambda_0$ and $a = 5\lambda_0$. All the interferers lie on the same azimuthal cut and are impinging from deterministic directions, equispaced between $-180°$ and 180°. As expected, the SIR decreases by increasing the number of links. It is worth noting that the SIR decreases monotonically starting from a certain number

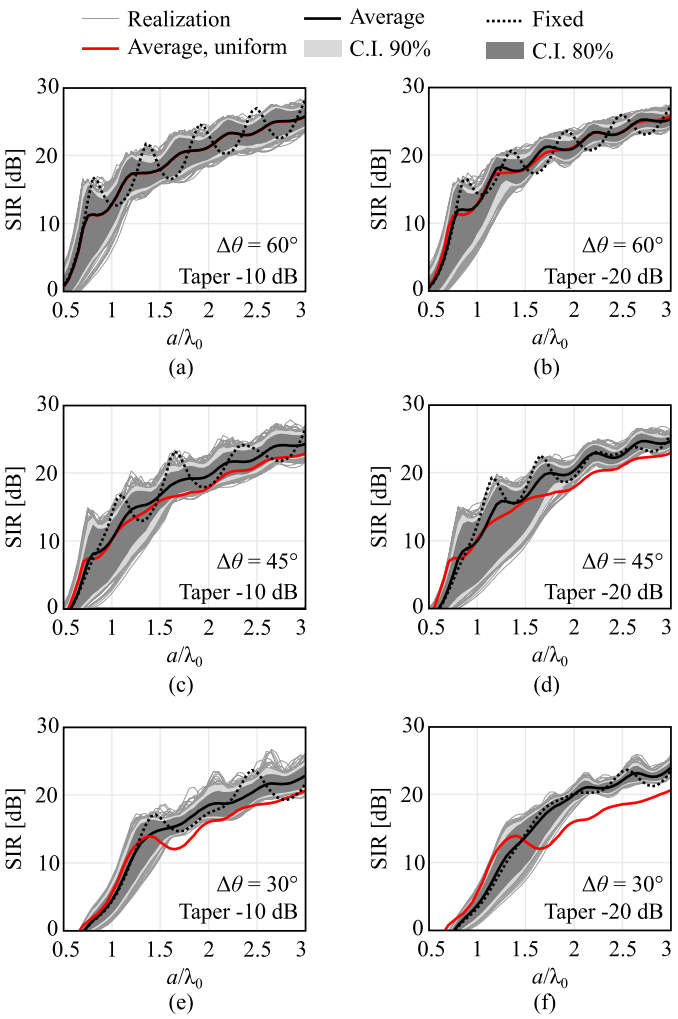

Fig. 11. SIR with the main beams oriented toward the desired user under the conditions of (a) 10 dB and (b) 20 dB Gaussian taper, both for $\Delta\theta = 60°$, (c) 10 dB, and (d) 20 dB Gaussian taper, for $\Delta\theta = 45°$, (e) 10 dB and (f) 20 dB Gaussian taper, for $\Delta\theta = 30°$.

of links corresponding to a spacing $\Delta\theta$ equal to the angular position of the first null of the antenna radiation pattern. Beyond this limit, the interferers contribute directly to the main beam of the receiving antenna. For a small number of links, the field generated by the interferers interacts with the side lobes of the receiving antenna mainly, and tapering guarantees higher SIR values.

Fig. 13 shows the SIR versus the number of links for the same cases as Fig. 12, but for interferers assumed to be impinging from random directions within the predefined sectors. Due to the random positions of the interfering plane waves, a Monte Carlo analysis of the SIR based on 250 realizations has been carried out. The SIR corresponding to the fixed interferers is compared with the average SIR extracted from the statistical analysis and the 90% confidence interval.

From Fig. 13(a) and (b), relevant to a one wavelength radius sphere, it is apparent that the differences between the number of beams achievable with the tapered and non-tapered (benchmark) distributions are not significant. However, from Fig. 13(c) and (d), where the antenna volume is large

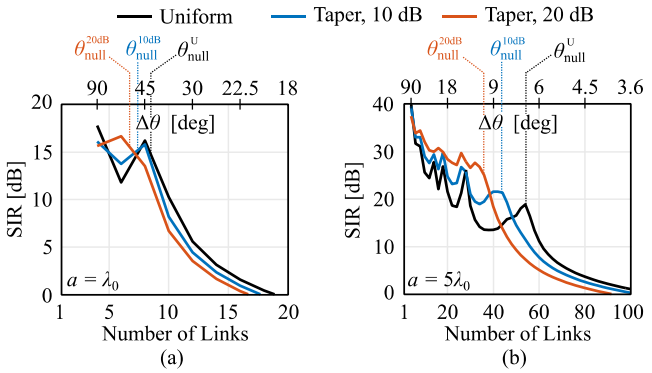

Fig. 12. SIR versus the number of realized links on the same azimuthal cut with a FoV = 360° and fixed interferers, for a radius (a) $a = \lambda_0$ and (b) $a = 5\lambda_0$.

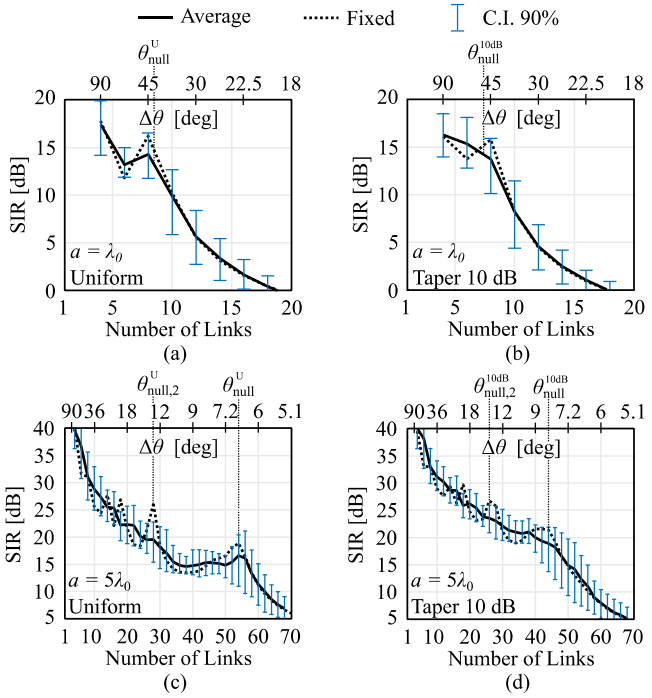

Fig. 13. SIR versus the number of realized links on the same azimuthal cut with a FoV = 360° and moving interferers, for a radius $a = \lambda_0$, and (a) uniform aperture distribution, (b) Gaussian taper of 10 dB, and for a radius $a = 5\lambda_0$ and (c) uniform aperture distribution, (d) Gaussian taper of 10 dB.

(i.e., $a = 5\lambda_0$) it is apparent that for $N_l < 50$, the tapering provides SIR higher than the benchmark (even 5 dB). The limit is dictated by the position of the first null and can be easily calculated with the approximate formula (14).

VI. Conclusion

An analysis of multi-beam antenna platforms for LoS mobile communications was provided. In particular, a new class of coefficients was introduced. They represent the coupling between the investigated patterns and the one associated with the observable field for the antenna platform of given dimensions. These coefficients can be used to evaluate the signal and the interference between beam-shaped links supported by the platform. Then, for the specific case of plane-wave-like links, a benchmark is established that allows estimating the maximum number of independent links that a platform can support. This benchmark is taken to be an antenna radiation pattern equal to the inward portion of the observable field. This choice guarantees that the signal from the desired users is maximized. Accordingly, any other solution for the pattern design can be compared to the benchmark to assess its merits. The observable field was calculated using the procedure based on the PO currents to examine the potential advantages of the benchmark. Two cases were investigated. For both, the users were tracked by a dedicated beam. The first case implied links between fixed equispaced interferers, while the second case regarded randomly distributed interferers within predefined angular sectors. The SIRs associated with the Gaussian distributions with 10 and 20 dB edge taper were compared to the benchmark. It resulted that, for fixed equispaced interferers, it is possible to exploit the maximum gain associated with the benchmark cases to achieve the maximum SIR at least over relatively narrow bands (10%–15%). However, for randomly distributed interferers, the advantage of the benchmark disappears, even for narrow bandwidths, when the antenna linear dimension is larger than $3\lambda_0$. In these cases, tapered distributions provide higher SIR.

Appendix A
Expression for the Received Power

The power received by the jth antenna, under impedance matching conditions, due to the ith impinging wave can be written as follows:

$$P_{\mathrm{r}}^{ij} = \frac{1}{8}\frac{\left|V_{oc}^{ij}\right|^2}{R_L^j} \tag{15}$$

where V_{oc}^{ij} is the open circuit voltage induced by the ith incident field, and R_L^j is the antenna load resistance. As suggested in [20], by multiplying the numerator and the denominator of (15) by the power P_{a}^j radiated by jth antenna, when fed by the current I_{a}^j, one obtains

$$P_{\mathrm{r}}^{ij} = \frac{P_{\mathrm{r}}^{ij}P_{\mathrm{a}}^j}{P_{\mathrm{a}}^j} = \frac{1}{8}\frac{\left|V_{oc}^{ij}\right|^2}{R_L^j}\frac{1}{2}\frac{R_L^j\left|I_{\mathrm{a}}^j\right|^2}{P_{\mathrm{a}}^j} = \frac{1}{16}\frac{\left|V_{oc}^{ij}I_{\mathrm{a}}^j\right|^2}{P_{\mathrm{a}}^j}. \tag{16}$$

Appendix B
Application of the Reciprocity Theorem

This Appendix is intended to prove (6), which relates $V_{oc}^{ij}I_{\mathrm{a}}^j$ with the reaction integral between the pattern of the inward observable field and the one that the receiving antenna would radiate when used in transmission. The starting point is the application of Lorentz's reciprocity theorem [23], [24], which gives

$$V_{oc}^{ij}I_{\mathrm{a}}^j = \oiint_{\mathbb{S}_f}\left(\vec{e}_{\mathrm{obs}}^{\,i}\times\vec{h}_{\mathrm{a}}^{\,j} - \vec{e}_{\mathrm{a}}^{\,j}\times\vec{h}_{\mathrm{obs}}^{\,i}\right)\cdot\hat{n}_f\,dS. \tag{17}$$

Although the steps leading to (17) are described in [23] and [24], we briefly report them here, revised to adapt to

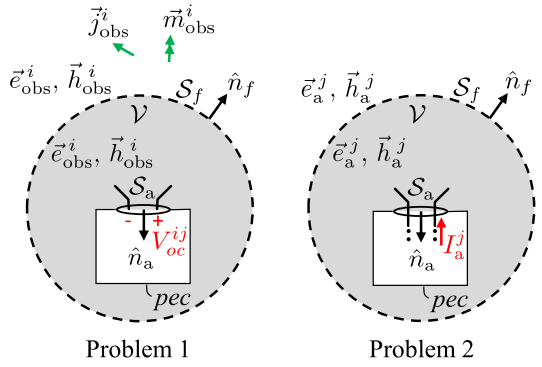

Fig. 14. Representation of Problem 1 and Problem 2 used in the reciprocity theorem.

the notation of this article. Please note that the formula of (17) is rigorously valid for any arbitrary incident field, however, here we assume that the only portion of the incident field that can interact with the receiving antenna is the observable field.

Fig. 14 shows an antenna enveloped by a surface $\mathcal{S}_f$, located in its far-field, and having the outer normal unit vector $\hat{n}_f$. The antenna is fed by a waveguide having the cross-section $\mathcal{S}_\mathrm{a}$, whose normal unit vector is $\hat{n}_a$. We define $\mathcal{V}$ as the volume comprised between $\mathcal{S}_f$, $\mathcal{S}_\mathrm{a}$, and the perfect electric conductor (pec) box, assumed to enclose the circuit connected to the antenna. Problem 1 refers to the receiving antenna, where the antenna terminals are open-circuited, while Problem 2 considers the same antenna when transmitting. In Problem 1, the observable field $\vec{e}^{\,i}_\mathrm{obs}$ and $\vec{h}^{\,i}_\mathrm{obs}$ is generated by the sources $\vec{j}^{\,i}_\mathrm{obs}$ and $\vec{m}^{\,i}_\mathrm{obs}$ located outside $\mathcal{V}$, inducing the open-circuit voltage V^{ij}_{oc} at the antenna terminals. Problem 2, where the antenna is assumed to be fed by the current I^j_a and radiates the fields $\vec{e}^{\,j}_\mathrm{a}$ and $\vec{h}^{\,j}_\mathrm{a}$, is a fictitious problem formulated to apply the reciprocity theorem. By applying Lorentz's reciprocity theorem to the volume $\mathcal{V}$, since no currents are contained within, one can write

$$\iint_{\mathcal{S}_a}\left(\vec{e}^{\,i}_\mathrm{obs}\times\vec{h}^{\,j}_\mathrm{a}-\vec{e}^{\,j}_\mathrm{a}\times\vec{h}^{\,i}_\mathrm{obs}\right)\cdot\hat{n}_\mathrm{a}dS + \oiint_{\mathcal{S}_f}\left(\vec{e}^{\,i}_\mathrm{obs}\times\vec{h}^{\,j}_\mathrm{a}-\vec{e}^{\,j}_\mathrm{a}\times\vec{h}^{\,i}_\mathrm{obs}\right)\cdot\hat{n}_f dS=0. \quad (18)$$

Being the antenna of Problem 1 open-circuited, the magnetic field $\vec{h}^{\,i}_\mathrm{obs}$ on $\mathcal{S}_\mathrm{a}$ has non-zero normal component solely, making the triple product $\vec{e}^{\,j}_\mathrm{a}\times\vec{h}^{\,i}_\mathrm{obs}\cdot\hat{n}_\mathrm{a}|_{\mathcal{S}_\mathrm{a}}$ vanish. Then, by assuming that in the waveguide only a single mode is supported, $\vec{e}^{\,i}_\mathrm{obs}$ and $\vec{h}^{\,j}_\mathrm{a}$ can be decomposed as

$$\vec{e}^{\,i}_\mathrm{obs}=V^{ij}_{oc}\vec{\mathfrak{e}}_0 \quad (19)$$

$$\vec{h}^{\,j}_\mathrm{a}=I^j_\mathrm{a}\vec{\mathfrak{h}}_0 \quad (20)$$

with $\vec{\mathfrak{e}}_0$ and $\vec{\mathfrak{h}}_0$ being the modal eigenvectors, and V^{ij}_{oc} and I^j_a their associated amplitudes. By substituting (19) and (20) in (18), one obtains

$$V^{ij}_{oc}I^j_\mathrm{a}\iint_{\mathcal{S}_\mathrm{a}}\vec{\mathfrak{e}}_0\times\vec{\mathfrak{h}}_0\cdot(-\hat{n}_\mathrm{a})dS = \oiint_{\mathcal{S}_f}\left(\vec{e}^{\,i}_\mathrm{obs}\times\vec{h}^{\,j}_\mathrm{a}-\vec{e}^{\,j}_\mathrm{a}\times\vec{h}^{\,i}_\mathrm{obs}\right)\cdot\hat{n}_f dS. \quad (21)$$

According to the orthonormality property of the eigenvectors $\vec{\mathfrak{e}}_0$ and $\vec{\mathfrak{h}}_0$, the integral in the left hand of (21) is equal to one, thus proving (17).

Since $\mathcal{S}_f$ is in the far-field, the fields $\vec{e}^{\,j}_\mathrm{a}(\vec{r}),\vec{h}^{\,j}_\mathrm{a}(\vec{r})$ radiated by the antenna can be rewritten as follows:

$$\vec{e}^{\,j}_\mathrm{a}(\vec{r})=\vec{V}^{\,j}_\mathrm{a}(\hat{k})\frac{e^{-jkr}}{r}$$

$$\vec{h}^{\,j}_\mathrm{a}(\vec{r})=\frac{1}{\zeta}\hat{r}\times\vec{V}^{\,j}_\mathrm{a}(\hat{k})\frac{e^{-jkr}}{r} \quad (22)$$

and the observable field as

$$\vec{e}^{\,i}_\mathrm{obs}(\vec{r})=\vec{V}^{\,i,\mathrm{inw}}_\mathrm{obs}(\hat{k})\frac{e^{jkr}}{r}+\vec{V}^{\,i,\mathrm{out}}_\mathrm{obs}(\hat{k})\frac{e^{-jkr}}{r},$$

$$\vec{h}^{\,j}_\mathrm{a}(\vec{r})=\frac{1}{\zeta}\hat{r}\times\left(-\vec{V}^{\,i,\mathrm{inw}}_\mathrm{obs}(\hat{k})\frac{e^{jkr}}{r}+\vec{V}^{\,i,\mathrm{out}}_\mathrm{obs}(\hat{k})\frac{e^{-jkr}}{r}\right). \quad (23)$$

By substituting (22) and (23) into (21), and omitting the $\hat{k}$ dependence of the patterns for compactness, one obtains

$$V^{ij}_{oc}I^j_\mathrm{a}=\frac{1}{\zeta}\oiint_{\mathcal{S}_f}\frac{1}{r^2}\Big[\left(\vec{V}^{\mathrm{inw}}_\mathrm{obs}+\vec{V}^{\mathrm{out}}_\mathrm{obs}e^{-2jkr}\right)\times\left(\hat{r}\times\vec{V}^{\,j}_\mathrm{a}\right)+ -\vec{V}^{\,j}_\mathrm{a}\times\left(\hat{r}\times\left(-\vec{V}^{\mathrm{inw}}_\mathrm{obs}+\vec{V}^{\mathrm{out}}_\mathrm{obs}e^{-2jkr}\right)\right)\Big]\cdot\hat{n}_f dS. \quad (24)$$

By expanding the vector triple products in (24), we can notice that the terms containing $\vec{V}^{\mathrm{out}}_\mathrm{obs}$ cancel out, while the ones containing $\vec{V}^{\mathrm{inw}}_\mathrm{obs}$ sum up. Thus, the expression simplifies as follows:

$$V^{ij}_{oc}I^j_\mathrm{a}=\frac{2}{\zeta}\oiint_{\mathcal{S}_f}\frac{1}{r^2}\vec{V}^{\mathrm{inw}}_\mathrm{obs}(\hat{k})\cdot\vec{V}^{\,j}_\mathrm{a}(\hat{k})\hat{r}\cdot\hat{n}dS. \quad (25)$$

By assuming that $\mathcal{S}_f$ is a sphere centered at the antenna reference system, $\hat{r}\cdot\hat{n}dS/r^2=d\hat{k}$, leading the integration on the solid angle [i.e., (6)]

$$V^{ij}_{oc}I^j_\mathrm{a}=\frac{2}{\zeta}\iint_{4\pi}\vec{V}^{\mathrm{inw}}_\mathrm{obs}(\hat{k})\cdot\vec{V}^{\,j}_\mathrm{a}(\hat{k})d\hat{k}. \quad (26)$$

Note that on the left-hand side of (26), neither V^{ij}_{oc} nor I^j_a is conjugated, as it derives from Lorentz's reciprocity theorem. Despite the product $V^{ij}_{oc}I^j_\mathrm{a}$ being dimensionally a power, it configures itself as a reaction [21] and relates quantities (V^{ij}_{oc} and I^j_a), associated with different sources of two separate problems.

ACKNOWLEDGMENT

The authors would like to thank Dr. Ulrik Imberg of HUAWEI Technologies Sweden AB Kista, Sweden for the fruitful discussion.

REFERENCES

[1] J. G. Andrews, T. Bai, M. N. Kulkarni, A. Alkhateeb, A. K. Gupta, and R. W. Heath, Jr., "Modeling and analyzing millimeter wave cellular systems," *IEEE Trans. Commun.*, vol. 65, no. 1, pp. 403–430, Jan. 2017.

[2] T. Schneider, A. Wiatrek, S. Preußler, M. Grigat, and R.-P. Braun, "Link budget analysis for terahertz fixed wireless links," *IEEE Trans. Terahertz Sci. Technol.*, vol. 2, no. 2, pp. 250–256, Mar. 2012.

[3] N. Llombart, D. Emer, M. Arias Campo, and E. McCune, "Fly's eye spherical antenna system for future Tbps wireless communications," presented at the Eur. Conf. Antennas Propag., Paris, France, Mar. 2017.

[4] M. Arias Campo, D. Blanco, S. Bruni, A. Neto, and N. Llombart, "On the use of fly's eye lenses with leaky-wave feeds for wideband communications," *IEEE Trans. Antennas Propag.*, vol. 68, no. 4, pp. 2480–2493, Apr. 2020.

[5] K. S. Rao, G. A. Morin, M. Q. Tang, S. Richard, and K. K. Chan, "Development of a 45 GHz multiple-beam antenna for military satellite communications," *IEEE Trans. Antennas Propag.*, vol. 43, no. 10, pp. 1036–1047, Oct. 1995.
[6] S. K. Rao, "Design and analysis of multiple-beam reflector antennas," *IEEE Antennas Propag. Mag.*, vol. 41, no. 4, pp. 53–59, Aug. 1999.
[7] S. K. Rao, C. C. Hsu, and K. K. Chan, "Antenna system supporting multiple frequency bands and multiple beams," *IEEE Trans. Antennas Propag.*, vol. 56, no. 10, pp. 3327–3329, Oct. 2008.
[8] N. Llombart, A. Neto, G. Gerini, M. Bonnedal, and P. De Maagt, "Leaky wave enhanced feed arrays for the improvement of the edge of coverage gain in multibeam reflector antennas," *IEEE Trans. Antennas Propag.*, vol. 56, no. 5, pp. 1280–1291, May 2008.
[9] T. N. Kaifas, D. G. Babas, G. Toso, and J. N. Sahalos, "Multibeam antennas for global satellite coverage: Theory and design," *IET Microw., Antennas Propag.*, vol. 10, no. 14, pp. 1475–1484, Nov. 2016.
[10] B. Biscontini, A. Murillo, J. Segador, and I. Gonzalez, "Active antenna architectures for enhanced 5G system performance," in *Proc. 14th Eur. Conf. Antennas Propag. (EuCAP)*, Copenhagen, Denmark, Mar. 2020, pp. 1–5.
[11] O. M. Bucci and G. Franceschetti, "On the degrees of freedom of scattered fields," *IEEE Trans. Antennas Propag.*, vol. 37, no. 7, pp. 918–926, Jul. 1989.
[12] P.-S. Kildal, E. Martini, and S. Maci, "Degrees of freedom and maximum directivity of antennas: A bound on maximum directivity of nonsuperreactive antennas," *IEEE Antennas Propag. Mag.*, vol. 59, no. 4, pp. 16–25, Aug. 2017.
[13] C. Ehrenborg and M. Gustafsson, "Physical bounds and radiation modes for MIMO antennas," *IEEE Trans. Antennas Propag.*, vol. 68, no. 6., pp. 4302–4311, Jun. 2020.
[14] C. Ehrenborg, M. Gustafsson, and M. Capek, "Capacity bounds and degrees of freedom for MIMO antennas constrained by Q-factor," *IEEE Trans. Antennas Propag.*, vol. 69, no. 9, pp. 5388–5400, Sep. 2021.
[15] S. Stein, "On cross coupling in multiple-beam antennas," *IRE Trans. Antennas Propag.*, vol. 10, no. 5, pp. 548–557, Sep. 1962.
[16] A. Neto, N. Llombart, and A. Freni, "The observable field for antennas in reception," *IEEE Trans. Antennas Propag.*, vol. 66, no. 4, pp. 1736–1746, Apr. 2018.
[17] A. Neto, A. F. Bernardis, D. Emer, A. Freni, and N. Llombart, "The observable field in complex scattering scenarios," *IEEE Trans. Antennas Propag.*, vol. 68, no. 7, pp. 5544–5555, Jul. 2020.
[18] R. F. Harrington, "On the gain and beamwidth of directional antennas," *IEEE Trans. Antennas Propag.*, vol. AP-6, no. 3, pp. 219–225, Jul. 1958.
[19] D.-H. Kwon and D. M. Pozar, "Optimal characteristics of an arbitrary receive antenna," *IEEE Trans. Antennas Propag.*, vol. 57, no. 12, pp. 3720–3727, Dec. 2009.
[20] V. Rumsey, "On the design and performance of feeds for correcting spherical aberration," *IEEE Trans. Antennas Propag.*, vol. AP-18, no. 3, pp. 343–351, May 1970.
[21] V. H. Rumsey, "Reaction concept in electromagnetic theory," *Phys. Rev.*, vol. 94, no. 6, pp. 1483–1491, Jun. 1954.
[22] P. F. Goldsmith, "Radiation patterns of circular apertures with Gaussian illumination," *Int. J. Infr. Millim. Waves*, vol. 8, no. 7, pp. 718–771, Jul. 1987.
[23] J. van Bladel, *Electromagnetic Fields*, 2nd ed. Hoboken, NJ, USA: Wiley, 2007.
[24] A. T. De Hoop, "The N-port receiving antenna and its equivalent electrical network," *Philips Res. Rep.*, vol. 30, pp. 302–315, 1975.

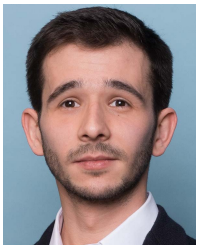

Riccardo Ozzola (Graduate Student Member, IEEE) received the B.Sc. and M.Sc. degrees (Hons.) from the University of Florence, Florence, Italy, in 2017 and 2019, respectively. His master thesis project was carried out at the Terahertz Sensing Group, Delft University of Technology (TU Delft), Delft, The Netherlands. He is currently pursuing the Ph.D. degree with TU Delft.

His current research interests include the theory and design of multi-beam wideband arrays for wireless communications, the electromagnetic characterization of multiple-input and multiple-output (MIMO) systems, and the development of numerical methods for electromagnetics.

Mr. Ozzola was one of the finalists for the Best Electromagnetics Paper Award at the European Conference on Antennas and Propagation (EuCAP) in 2021.

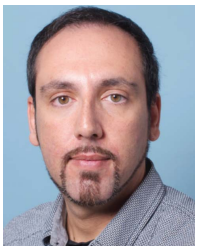

Daniele Cavallo (Senior Member, IEEE) received the M.Sc. degree (*summa cum laude*) in telecommunication engineering from the University of Sannio, Benevento, Italy, in 2007, and the Ph.D. degree (*cum laude*) in electromagnetics from the Eindhoven University of Technology, Eindhoven, The Netherlands, in 2011.

From 2007 to 2011, he was with the Antenna Group, Netherlands Organization for Applied Scientific Research, The Hague, The Netherlands. From 2012 to 2015, he was a Post-Doctoral Researcher with the Microelectronics Department, Delft University of Technology (TU Delft), Delft, The Netherlands. In 2015, he joined the Chalmers University of Technology, Gothenburg, Sweden, as a Visiting Researcher. He is currently an Associate Professor with the Terahertz Sensing Group, TU Delft. He has authored or coauthored more than 150 papers published in peer-reviewed international journals and conference proceedings. His current research interests include analytical and numerical methods for antenna characterization, the design of antenna arrays, and on-chip antennas.

Dr. Cavallo is a member of the European Association on Antennas and Propagation (EurAAP), a co-coordinator of the EurAAP working group "Active Array Antennas," and a Management Committee Member of the COST Action "Future communications with higher-symmetric engineered artificial materials (SyMat)." He was a recipient of the Best Innovative Paper Prize at the European Space Agency Antenna Workshop in 2008, the Best Paper Award in Electromagnetics and Antenna Theory at the 11th European Conference on Antennas and Propagation (EuCAP) in 2017, and the 250 keuro "Veni" Personal Grant from the Netherlands Organization for Scientific Research (NW0) in 2015. His students received the Best Student Paper Award at EuCAP 2013, the Special Mention at EuCAP 2015, the Else Kooi Prize in 2016, and the Honorable Mention at the IEEE Antennas and Propagation Society International Symposium in 2019. He is currently an Associate Editor of the IEEE TRANSACTIONS ON ANTENNAS AND PROPAGATION.

Angelo Freni (Senior Member, IEEE) received the Laurea (Doctors) degree in electronics engineering from the University of Florence, Florence, Italy, in 1987.

In 1994, he was involved in research with the Engineering Department, University of Cambridge, Cambridge, U.K., concerning the extension and the application of the finite element method to the electromagnetic scattering from periodic structures. From 1995 to 1999, he was an Adjunct Professor with the University of Pisa, Pisa, Italy. Between 2009 and 2010, he also spent one year as a Researcher at the TNO Defence, Security, and Safety, The Hague, The Netherlands, focused on the electromagnetic modeling of kinetic inductance devices and their coupling with an array of slots in the terahertz range. Since 1990, he has been with the Department of Electronic Engineering, University of Florence, first as an Assistant Professor and from 2002 as an Associate Professor of electromagnetism; in 2014 he obtained the Full Professor qualification. Since 2012, he has been a Visiting Professor with the TU Delft University of Technology, Delft, The Netherlands. His current research interests include meteorological radar systems, radiowave propagation, numerical and asymptotic methods in electromagnetic scattering and antenna problems, electromagnetic interaction with moving media, and remote sensing. In particular, part of his research concerned numerical techniques based on the integral equation, with a focus on domain decomposition and fast solution methods.

Nuria Llombart (Fellow, IEEE) received the master's degree in electrical engineering and the Ph.D. degree from the Polytechnic University of Valencia, Valencia, Spain, in 2002 and 2006, respectively.

During the master's studies, she spent one year with the Friedrich Alexander University of Erlangen Nuremberg, Erlangen, Germany, and worked at the Fraunhofer Institute for Integrated Circuits, Erlangen. From 2002 to 2007, she was with the Antenna Group, TNO Defence, Security and Safety Institute, The Hague, The Netherlands, as a Ph.D. Student and then as a Researcher. From 2007 to 2010, she was a Post-Doctoral Fellow with the California Institute of Technology, working with the Submillimeter Wave Advance Technology Group, Jet Propulsion Laboratory, Pasadena, CA, USA. From 2010 to 2012, she was a Ramón y Cajal Fellow with the Optics Department, Complutense University of Madrid, Madrid, Spain. In September 2012, she joined the THz Sensing Group, Technical University of Delft, Delft, The Netherlands, where she has been a Full Professor since February 2018. She has coauthored more than 200 journal and international conference contributions in the areas of antennas and THz systems.

Dr. Llombart was a co-recipient of the H. A. Wheeler Award for the Best Applications Paper of 2008 in IEEE TRANSACTIONS ON ANTENNAS AND PROPAGATION, the 2014 THz Science and Technology Best Paper Award of the IEEE Microwave Theory and Techniques Society, and several NASA awards. She was also a recipient of the 2014 IEEE Antenna and Propagation Society Lot Shafai Mid-Career Distinguished Achievement Award. She serves as a Board Member for the IRMMW-THz International Society and an Associate Editor of IEEE TRANSACTIONS ON ANTENNAS AND PROPAGATION. In 2015, she was a recipient of a European Research Council Starting Grant. In 2019, she became an IEEE Fellow for contributions to the millimeter- and submillimeter-wave quasi-optical systems.

Andrea Neto (Fellow, IEEE) received the Laurea degree (*summa cum laude*) in electronic engineering from the University of Florence, Florence, Italy, in 1994, and the Ph.D. degree in electromagnetics from the University of Siena, Siena, Italy, in 2000. Part of his Ph.D. degree was developed at the European Space Agency Research and Technology Centre, Noordwijk, The Netherlands.

He was with the Antenna Section, European Space Agency Research and Technology Centre, Noordwijk, for over two years. From 2000 to 2001, he was a Post-Doctoral Researcher with the California Institute of Technology, Pasadena, CA, USA, where he was with the Submillimeter Wave Advanced Technology Group. From 2002 to 2010, he was a Senior Antenna Scientist with the Netherlands Organization for Applied Scientific Research Defence, Security, and Safety, The Hague, The Netherlands. In 2010, he became a Full Professor of applied electromagnetism with the Department of Microelectronics, Delft University of Technology, Delft, The Netherlands, where he formed and currently leads the THz Sensing Group. His current research interests include the analysis and design of antennas with an emphasis on arrays, dielectric lens antennas, wideband antennas, EBG structures, and THz antennas.

Dr. Neto is a member of the Technical Board of the European School of Antennas and an Organizer of the course on antenna imaging techniques. He is a member of the Steering Committee of the Network of Excellence NEWFOCUS, dedicated to focusing on techniques in millimeter- and submillimeter-wave regimes. He was a recipient of the European Research Council Starting Grant to perform research on advanced antenna architectures for terahertz sensing systems in 2011, the H. A. Wheeler Award for the Best Applications Paper in the IEEE TRANSACTIONS ON ANTENNAS AND PROPAGATION in 2008, the Best Innovative Paper Prize of the European Space Agency Antenna Workshop in 2008, and the Best Antenna Theory Paper Prize of the European Conference on Antennas and Propagation in 2010. He served as an Associate Editor for the IEEE TRANSACTIONS ON ANTENNAS AND PROPAGATION from 2008 to 2013 and the IEEE ANTENNAS AND WIRELESS PROPAGATION LETTERS from 2005 to 2013.